Tidal currents of the Ross Sea and their time stability

ERIC S. JOHNSON[1]* and MICHAEL L. VAN WOERT[2]*

[1]*Earth and Space Research, 1910 Fairview Ave. E. Suite 210, Seattle, WA 98102, USA*
[2]*National Science Foundation, Office of Polar Programs, 4201 Wilson Blvd, Arlington, VA 22230, USA*
*ejohnson@esr.org

Abstract: Current measurements obtained from a sparse array of moorings on the Ross Continental Shelf during the 1980 and 90s are analysed for their tidal constituents. Diurnal (K_1 and O_1) tides are about five times stronger than semi-diurnal tides, and are strongest near the shelf break in agreement with recent model results. At some energetic locations the diurnal tides are significantly weaker at depth, presumably due to bottom friction. Complex demodulation analysis shows that at some locations the tidal response varies significantly in time. This time variability rises markedly above the noise floor expected from the spectral continuum between tidal bands, and does not scale with tidal bandwidth as would be expected of broadband noise. Further its magnitude is generally proportional to the associated tidal constituent, indicating that it is truly a varying tidal response. Space scales of this tidal instability were not resolved but are less than 150 km, while time scales appear mostly seasonal to interannual. The rms magnitude of the unstable response can be 1/3 of a given component's mean magnitude, placing substantial limits on the ability of prognostic or even data assimilative models to accurately predict these tides for any specific time period.

Introduction

The basic theory of astronomically forced tides was first described over one hundred years ago. With recent measurements from altimetric satellites (Cartright & Ray 1990) the major tidal constituents over much of the open ocean are now well known. Facilitated by recent increases in computing power and improved maps of bottom bathymetry, and by assimilation techniques for altimetric data, increasingly realistic open-ocean tidal models are becoming available (e.g. Le Provost *et al.* 1998, Lefevre 2002). Over the continental shelves tides are believed to play a significant role in ocean mixing (Munk & Wunsch 1998). This is especially true over the Antarctic continental shelf where tidal mixing has been implicated as one possible mechanism for the formation of High Salinity Shelf water (Foldvik *et al.* 1985), which is itself an important ingredient of Antarctic Bottom Water.

Tides have been extensively studied in McMurdo Sound (Lewis & Perkin 1985, Barry & Dayton 1988), along the Ross Ice Shelf (Pillsbury & Jacobs 1985), and under the Ross Ice Shelf (Williams & Robinson 1980, MacAyeal 1984, 1985). These later studies have primarily focused on the tidally induced basal melting at the bottom of the floating Ross Ice Shelf. Tides in the Ross Sea may also be important in biological processes by

1) transporting material in tidally rectified bottom currents (Loder 1980, MacAyeal 1985, Dunbar *et al.* 1985), and

2) by mixing nutrients within the water column (e.g. Crawford 1991).

Tides have not been well described over most of Ross Sea continental shelf region. The data that exist indicate that tidal currents are a dominant feature of the circulation - often many times stronger than the long-term circulation. Recent attempts at developing tidal models for the Antarctic continental shelf (e.g. Robertson *et al.* 2003, Padman *et al.* 2003) have been hampered by the lack of data with which to constrain and validate the models. We support these modelling studies by providing a comprehensive tidal analysis of the available current meter data from the Ross Sea.

Previous studies have also shown that the ocean's tidal response to astronomical forcing is not completely steady with time. Foldvik *et al.* (1990) have demonstrated that the K_1 and M_2 tidal amplitudes vary seasonally in the Weddell Sea. Cummins *et al.* (2000) found similar seasonal effects in the tides propagating along the shelf of Vancouver Island and, with model simulations, demonstrated the source to be seasonal variations in large-scale stratification and currents. Growing interest in the use of models to remove tides from synoptic current surveys (e.g. Erofeeva *et al.* 2005) require quantitative answers to the question of how stable the tidal response is with time, since models tuned to replicate current meter data over many years might be used to remove tides from a survey taken in a specific month. Thus we further analyse the current meter data to address the temporal stability of the ocean tidal components.
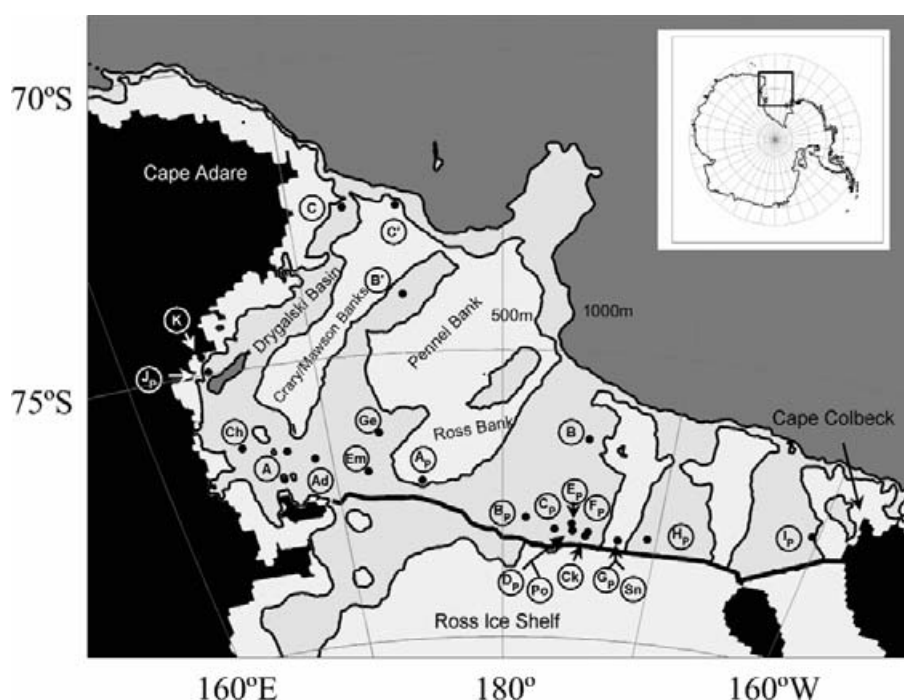
Fig. 1. The Ross Sea study area. The locations of the A'/Adélie (Ad), Chinstrap (Ch), Gentoo (Ge), Emperor (Em), B', C', RSFE A B & C (A B C), K, Prism A-J (AP-JP), Snap (Sn), Crackle (Ck), and Pop (Po) moorings are indicated. Depth contours are 500 and 1000 m.

Data and methods

Topographically, the Ross Sea continental shelf is extremely broad, in places exceeding 500 km in width. The shelf is oriented in a north-west–south-east direction between Cape Adare (72°S, 170°E) and Cape Colbeck (77.5°S, 158°W). It has a generally flat bottom near the dateline, but is punctuated by a series of trenches and rises toward the west that connect the near coastal regions to the continental slope. The mean water depth on the shelf is about 500 m (Carmack 1977), but it varies from 1200 m in the Drygalski Basin to less than 300 m on the Crary/Mawson and Pennel banks (Fig. 1).

We perform a harmonic tidal analysis on all available data, which includes data from recent programs as well as records from the WOCE current meter archive at Oregon State University. However, the time stability analysis is restricted to data from two Italian, three United States, and one joint Italian/United States current meter moorings set in the Ross Sea between December 1996 and December 1998 as part of the US Research on Ocean Atmospheric Variability and Ecosystem Response in the Ross Sea (ROAVERRS) and Italian Biogenic Sedimentation in the Southern Ocean (BIOSESO) programs. All of the moorings were taut line, subsurface moorings, with near surface instruments deployed on four of the moorings. The locations of the moorings (Fig. 1) as well as other pertinent information on the moorings and instruments are provided in Table I. Three moorings were located in the northern part of the Ross Sea. Mooring B' was set in the Joides Basin in water 588 m deep. The basin is bounded on the west by Crary and Mawson banks and on the east by Pennell Bank (Fig. 1). The GEBCO map (Vanney & Johnson 1985) shows

the basin to be at least partially obstructed to the north by Scott Shoal. Mooring C' was set to the north right on the shelf break, while the Ross Sea Flux Experiment C mooring (RSFE-C) was set some 10 km back. A second grouping of moorings were deployed to the south near the Ross Ice Shelf. Emperor and Gentoo were in the Ross Sea Polynya

Table I. Ross Sea mooring names, locations, and water depths for which data is available in the 1980s and 1990s.

Mooring Indentifier	Latitude (°N)	Longitude (°E)	Depth (m)
Prism-I	-77.680	-160.403	590
Prism-H	-78.163	-170.612	558
Snap	-78.227	-172.490	420
Prism-G	-78.220	-172.518	443
Snap 3	-78.192	-172.800	436
Prism-F	-78.108	-174.513	567
Crackle	-78.183	-174.650	530
RSFE-B	-76.497	-174.993	569
Pop	-78.092	-175.500	489
Prism-D	-78.098	-175.503	558
Prism-E	-77.978	-175.597	585
Prism-C	-78.078	-176.658	595
Prism-B	-77.882	-178.533	700
Prism-A	-77.207	175.155	685
B'	-74.000	175.000	588
C'	-72.500	175.000	456
Gentoo	-76.339	172.936	620
RSFE-C	-72.480	172.525	533
Emperor	-76.982	171.979	671
A'/Adélie	-76.683	169.017	810
RSFE-A	-76.502	167.500	775
Chinstrap	-76.341	165.030	828
Prism-J	-74.965	164.393	879
K	-74.700	164.250	554

Table II. The major diurnal and semi-diurnal tidal constituents.

	Darwin symbol	Constituent name	Period (hr)
Diurnal	Q_1	Elliptical lunar	26.868
	O_1	Principal lunar	25.819
	P_1	Principal solar	24.066
	K_1	Declination luni-solar	23.934
Semi-diurnal	N_2	Elliptical lunar	12.658
	M_2	Principal lunar	12.421
	S_2	Principal solar	12.000
	K_2	Declination luni-solar	11.967

for most of their duration, while A'/Adélie and Chinstrap were located to the west. A complete description of the Ross Sea current meter program can be found in Van Woert *et al.* (2003), along with discussion of the seasonal and longer-period currents.

Estimates of the time-averaged tidal currents at each site were established from the year-long current meter records using harmonic analysis (Foreman 1978) of data subsampled to hourly intervals. In order to maintain a common base period for analysis, generally only data for the period February 1998 through November 1998 (7272 hours) were included in the tidal analysis. Data from site K and the deep instrument at site B were only available for the previous year; therefore, data from these sites were also analysed for the period February 1997 through November 1997. The tidal software package by default incorporates 69 constituents in the analysis. Nevertheless because none of the records exceeded a year in length the SA, PI1, PSI1, GAM_2 and other constituents were not resolvable by the analysis using a standard Rayleigh criterion of 1.0 (Forman 1977). We report the four major constituents for both the diurnal and semi-diurnal tides (Table II).

The stability of the tidal response over time was estimated using complex demodulation (Tsai *et al.* 1992) of the processed, half-hourly data. We prefer this continuous, time series technique over the common resort of chopping data into segments and preforming a piecewise harmonic analysis for several reasons. First, the signal we seek is in fact continuously varying and requires us to make careful choices that balance time resolution against frequency resolution: the results of these choices are most explicit and flexible in continuous techniques. Second, we seek not only the analysed tide's time variability but also how confidently we can attribute this variability to either a changing tidal response or to the background noise continuum. Such problems are widely encountered in spectral analysis and the techniques there well developed; but the question cannot be addressed in a piecewise analysis for lack of detailed resolution of the spectra in the vicinity of tidal peaks. We therefore use complex demodulation for all aspects of the tidal stability analysis.

In complex demodulation one essentially Fourier transforms the data into the frequency domain, retaining the

full frequency resolution allowed by the time series. One then selects the desired frequency band, generally centred on the frequency of interest, which is equivalent to band pass filtering the original time series. The selected Fourier components (each a complex exponential) are then divided by a unit sinusoid of the desired centre frequency, which shifts the entire frequency band to centre about zero frequency: this is the essence of demodulation, since now all variability is cast in terms of modifications to the chosen unit sinusoid just as the original Fourier coefficients represented departures from the mean. We then re-transform the shifted Fourier coefficients back to the time domain to complete the demodulation process:

$$D(t) = \int_{f_0-\Delta f/2}^{f_0+\Delta f/2} e^{i(f-f_0)t} \left[\frac{\sqrt{2}}{T} \int_0^T u(\tau)e^{-if\tau} d\tau \right] df, \quad (1)$$

where the factor of $\sqrt{2}$ restores variance lost when negative frequencies are neglected in the transform back to the time domain. The resulting complex time series D consists of the amplitude and phase of the band-passed time series u as normalized by a sinusoid of the chosen centre frequency f_0. For example data containing a pure sinusoid of the centre frequency will demodulate into a complex constant (which is simply the zero frequency of the inverse transform) whose magnitude is the RMS amplitude of the original time series. The presence of other frequencies in the original band will contribute slow changes to the demodulated series, both in magnitude and phase, showing how the original time series departs from the centre sinusoid. The rate of this modulation will of course depend on the inverse bandwidth of the retained signal. The band-passed signal itself can be recovered by restoring the modulation frequency:

$$u_b(t) = \mathrm{Re}\left[D(t)e^{if_0 t} \right] \quad (2)$$

Note that for discreet data the transform Eq. (1) can only be accomplished for f_0 some multiple of $1/T$: one corrects the resulting D to the exact tidal frequency by simply adding a small time trend of phase representing the frequency mismatch between the tide and f_0.

Since the original band-passed Fourier coefficients have two degrees of freedom per retained frequency their resulting demodulated time series has a time resolution of half the inverse bandwidth. The actual response function in time will be a sinc function with width (between zero crossings) equal to the inverse bandwidth. Note that since demodulation is a spectral technique it requires continuous data. We linearly interpolated across the short gaps between mooring deployments, and filled larger gaps with the time series mean. This creates periods of zero tidal amplitude in the resulting demodulated time series; we reset these gap periods to undefined in the demodulated series, along with a full time resolution's width of data to either side, so that

Table III. Major diurnal tidal constituents for Ross Sea moorings derived from harmonic analysis.

Mooring name	Inst. Depth (m)	Q1 Major Axis (A) (cm s⁻¹)	Q1 Minor Axis (B) (cm s⁻¹)	Q1 Incl (°T)	Q1 ϑ (°)	O1 Major Axis (A) (cm s⁻¹)	O1 Minor Axis (B) (cm s⁻¹)	O1 Incl (°T)	O1 ϑ (°)	P1 Major Axis (A) (cm s⁻¹)	P1 Minor Axis (B) (cm s⁻¹)	P1 Incl (°T)	P1 ϑ (°)	K1 Major Axis (A) (cm s⁻¹)	K1 Minor Axis (B) (cm s⁻¹)	K1 Incl (°T)	K1 ϑ (°)	Rec. Leng. (days)
Prism-I	255	0.25	0.01	4	164	1.55	0.01	355	200	0.48	-0.11	347	218	1.39	-0.17	346	224	370
	540	0.27	-0.17	33	170	1.42	-0.39	342	177	0.51	-0.06	342	228	1.49	-0.14	329	221	370
Prism-H	305	0.41	-0.14	324	224	2.32	-0.49	318	218	0.82	0.23	320	233	3.14	0.64	329	220	372
Snap	211	0.28	-0.13	88	3	0.99	-0.08	340	220	0.91	0.11	358	197	2.02	0.06	356	223	354
	383	0.59	-0.19	312	209	2.82	-0.47	327	210	1.25	0.21	337	223	4.62	-0.06	342	220	354
Prism-G	215	0.63	-0.26	318	182	3.30	-0.76	327	206	1.56	0.06	333	215	5.42	0.09	338	214	374
	395	0.57	-0.22	312	174	3.22	-0.65	328	206	1.58	0.07	339	215	5.23	0.21	341	219	374
Snap-3	240	0.51	-0.08	318	180	2.47	-0.48	325	189	1.55	-0.05	339	210	3.65	0.14	336	205	643
Prism-F	210	0.84	-0.12	313	236	3.31	-0.82	319	242	1.42	0.06	326	252	4.94	0.27	324	252	374
	285	0.75	-0.19	318	232	3.21	-0.83	321	243	1.40	0.08	331	251	4.72	0.31	327	252	374
Crackle	237	0.31	-0.22	320	243	2.69	-0.81	308	249	1.05	0.20	315	260	3.98	0.04	309	260	354
	310	0.16	-0.11	7	239	0.97	-0.29	325	220	0.49	0.11	338	186	2.01	0.06	330	232	352
	492	0.32	-0.10	307	222	2.70	-0.34	300	243	1.24	0.07	301	256	3.78	0.32	303	261	354
RSFE-B	241	0.47	0.30	339	322	3.10	1.60	339	333	1.21	0.75	4	289	5.49	4.10	347	334	732
	534	0.60	0.14	46	337	0.88	0.40	58	158					5.09	3.23	22	347	106
Pop	253	0.42	-0.24	306	238	2.97	-0.92	309	248	1.28	0.08	314	259	4.32	0.38	319	264	353
	327	0.45	-0.11	312	259	2.76	-0.53	294	244	1.20	0.27	301	258	3.75	0.66	304	264	353
	508	0.32	0.14	340	196	1.81	-0.84	299	251	0.59	-0.03	303	263	2.47	0.28	312	274	353
Prism-D	125	0.64	-0.05	326	239	3.15	-0.75	318	247	1.42	0.11	316	258	4.61	0.44	327	259	375
	225	0.73	-0.10	323	240	2.99	-0.79	323	246	1.47	0.08	327	258	4.50	0.58	330	261	375
	300	0.62	-0.09	310	238	2.86	-0.76	309	244	1.51	0.09	316	257	4.25	0.16	317	267	375
Prism-E	210	0.59	-0.11	337	238	2.91	-0.79	327	246	1.39	0.04	329	262	4.58	0.46	332	260	376
	285	0.66	-0.07	324	240	2.81	-0.75	324	247	1.23	-0.04	330	260	4.47	0.42	327	259	376
	515	0.58	-0.09	312	230	2.71	-0.67	326	250	1.30	-0.05	332	263	4.31	0.36	330	264	376
Prism-C	425	0.51	-0.22	341	256	2.74	-0.81	327	259	1.23	-0.09	330	247	3.91	-0.07	328	266	310
Prism-B	425	0.52	-0.05	28	325	2.49	-0.91	345	280	1.16	-0.37	0	290	3.29	-0.38	343	290	268
	650	0.44	-0.28	341	272	2.79	-1.20	343	279	1.33	-0.19	339	292	3.97	-0.65	340	293	378
Prism-A	350	0.81	-0.22	43	304	2.55	-1.90	364	277	1.55	-0.40	9	305	4.09	-1.63	7	305	332
B'	220	1.11	0.17	330	318	5.79	0.22	329	308	3.61	0.74	325	352	11.40	2.06	325	356	1845
	555	0.96	0.12	341	318	5.03	0.02	338	305	3.34	0.56	333	346	9.77	1.45	334	353	1100
C'	230	5.38	4.61	44	196	40.15	31.88	43	237	13.62	10.33	26	323	41.85	31.42	31	322	398
	425	2.27	1.87	359	254	20.50	18.06	47	241	6.14	4.63	19	343	24.58	18.90	30	333	398
Gentoo	24	0.65	-0.12	338	272	2.92	-0.68	359	290	1.38	0.23	2	311	4.05	-0.04	351	317	335
	196	0.76	-0.35	324	258	3.40	-1.03	356	294	1.43	0.06	350	322	5.03	-0.14	348	323	335
	427	0.58	-0.12	338	273	2.67	-0.62	3	292	1.14	0.15	354	310	3.97	-0.16	353	319	335
	604	0.73	-0.05	3	282	2.62	-0.76	9	293	1.21	-0.11	0	316	3.82	-0.26	2	319	335
RSFE-C	241	1.59	1.41	324	37	17.54	10.93	338	49	4.48	3.24	3	109	17.32	11.27	352	126	414
	498	2.74	0.57	27	306	12.67	4.73	33	317	5.48	1.83	40	39	14.67	4.18	40	35	414
Emperor	107	0.58	-0.35	35	315	2.66	-0.84	345	276	1.43	-0.06	346	304	4.39	-0.01	346	307	700
	210	0.64	-0.36	23	294	2.82	-0.83	353	282	1.33	-0.11	351	305	4.13	-0.33	351	307	700
	497	0.69	-0.18	350	241	2.52	-0.73	349	277	1.14	0.02	1	310	3.89	-0.60	343	305	359
	657	0.44	-0.26	68	329	2.78	-0.95	356	276	1.57	-0.24	0	309	4.03	-0.45	351	310	333
A'/Adélie	40	0.38	-0.21	356	249	2.13	-0.67	352	268	0.95	-0.10	2	303	2.78	-0.42	352	305	702
	220	0.55	-0.22	351	267	2.34	-0.82	349	280	0.86	-0.23	344	310	3.10	-0.50	347	313	739
	770	0.44	-0.18	339	261	2.26	-0.81	354	282	0.95	-0.13	355	315	2.81	-0.42	354	314	2159
RSFE-A	241	0.18	-0.06	351	280	0.96	-0.22	343	289	0.39	0.00	349	316	1.16	-0.09	347	331	731
	740	0.17	-0.12	74	105	0.64	-0.21	280	315	0.13	-0.01	309	22	0.67	-0.16	295	7	648
Chinstrap	36	0.26	-0.04	357	227	1.72	0.05	355	252	0.74	0.04	346	288	2.14	0.04	358	287	356
	210	0.44	0.12	335	233	2.42	-0.17	349	260	0.93	0.03	355	296	3.11	0.01	353	298	703
	813	0.56	-0.24	13	247	2.58	-0.17	356	258	1.06	0.03	357	300	3.28	0.01	353	300	344
Prism-J	40	0.57	0.18	42	203	1.27	-0.17	45	263	0.71	0.15	18	283	1.83	-0.09	32	304	281
	780	0.35	-0.29	12	207	1.73	0.02	68	279	0.79	-0.20	20	274	1.78	-0.33	49	317	277
K	200	0.16	-0.05	18	4	0.42	-0.36	271	74	0.19	-0.12	37	251	0.38	-0.19	16	246	733

they are ignored in further analysis. This removes the major effects of gaps from the remaining data, though the remaining side-lobes can reach roughly 10% of the component amplitude. Still, since gaps occur no more than yearly this amounts to little rms variability, about 5.4% of the component amplitude for yearly one-month gaps.

Table IV. Semi-diurnal tidal constituents for Ross Sea moorings derived from harmonic analysis.

Mooring name	Inst. Depth (m)	N₂ Major Axis (A) (cm s⁻¹)	N₂ Minor Axis (B) (cm s⁻¹)	Incl (°T)	ϑ (°)	M₂ Major Axis (A) (cm s⁻¹)	M₂ Minor Axis (B) (cm s⁻¹)	Incl (°T)	ϑ (°)	S₂ Major Axis (A) (cm s⁻¹)	S₂ Minor Axis (B) (cm s⁻¹)	Incl (°T)	ϑ (°)	K₂ Major Axis (A) (cm s⁻¹)	K₂ Minor Axis (B) (cm s⁻¹)	Incl (°T)	ϑ (°)	Rec. Leng. (days)
Prism-I	255	0.93	0.05	7	103	0.87	0.12	2	187	1.23	0.03	8	116	0.40	-0.03	4	111	370
	540	0.94	0.03	334	105	0.70	-0.01	331	188	1.24	0.13	335	118	0.34	0.03	344	129	370
Prism-H	228					0.59	0.08	52	36	1.38	0.67	8	191					15
	305	0.53	0.06	354	171	0.40	-0.12	317	224	0.50	-0.03	15	183	0.21	0.01	354	203	372
Snap	211	0.33	-0.05	12	207	0.60	0.11	353	250	0.25	0.00	353	251	0.35	0.03	357	89	354
	383	0.41	-0.04	30	204	0.45	0.22	310	260	0.47	-0.07	18	206	0.09	-0.05	304	183	354
Prism-G	215	0.51	-0.08	26	196	0.39	0.15	326	224	0.50	-0.05	355	183	0.18	-0.03	298	218	374
	395	0.46	-0.06	17	189	0.34	0.09	329	250	0.53	0.06	22	213	0.23	0.04	296	197	374
Snap-3	240	0.12	0.06	14	204	0.17	0.01	341	233	0.14	-0.04	18	194	0.12	0.03	16	91	643
Prism-F	210	0.58	-0.05	348	177	0.36	-0.12	312	252	0.47	0.08	355	207	0.12	-0.02	336	140	374
	285	0.53	-0.04	349	182	0.45	-0.15	325	264	0.51	0.16	0	213	0.10	0.00	335	176	374
Crackle	237	0.39	-0.11	352	209	0.39	-0.12	313	217	0.42	-0.01	341	216	0.13	0.00	281	348	354
	310	0.20	0.04	386	212	0.14	-0.05	58	338	0.23	-0.05	356	176	0.29	0.10	16	156	352
	492	0.32	-0.01	346	210	0.50	-0.21	311	268	0.31	0.05	314	234	0.26	0.08	4	186	354
RSFE-B	241	0.21	0.12	13	352	0.36	0.30	39	355	0.38	0.22	6	15	0.32	0.17	36	214	732
	534	0.44	-0.08	342	121	0.89	-0.24	285	313	1.00	-0.20	80	35					106
Pop	253	0.22	-0.10	13	225	0.33	-0.05	329	251	0.48	0.04	345	209	0.14	-0.02	26	68	353
	327	0.18	-0.06	355	218	0.32	-0.22	296	238	0.36	0.08	311	213	0.20	-0.11	73	223	353
	508	0.16	-0.05	63	272	0.33	-0.20	352	264	0.13	-0.04	338	209	0.21	0.04	77	204	353
Prism-D	125	0.28	-0.10	9	212	0.40	-0.08	323	259	0.52	0.13	341	201	0.11	-0.05	349	177	375
	225	0.30	-0.06	16	223	0.42	-0.05	334	257	0.41	0.09	348	209	0.16	-0.03	23	193	375
	300	0.38	-0.05	2	238	0.45	-0.18	337	271	0.37	-0.03	348	237	0.21	0.02	9	153	375
Prism-E	210	0.40	-0.14	17	197	0.46	-0.10	311	245	0.41	0.03	11	212	0.13	0.01	10	199	376
	285	0.41	-0.07	8	198	0.33	-0.19	310	243	0.47	0.11	5	216	0.20	0.06	352	194	376
	515	0.37	0.05	30	217	0.35	-0.02	347	282	0.28	-0.07	36	241	0.15	0.09	42	278	376
Prism-C	425	0.34	0.00	6	228	0.38	-0.09	348	283	0.38	0.04	2	236	0.15	-0.02	341	211	310
Prism-B	425	0.37	0.09	13	233	0.41	0.16	0	292	0.34	-0.06	358	227	0.15	-0.10	299	243	268
	650	0.33	-0.06	360	208	0.36	-0.01	345	268	0.41	0.00	7	246	0.11	0.02	35	334	378
Prism-A	350	0.23	-0.07	43	230	0.28	0.02	23	203	0.38	-0.10	19	228	0.16	-0.07	315	287	332
B'	220	0.57	0.17	14	292	0.84	0.27	14	307	0.64	-0.05	21	336	0.73	0.36	79	173	1845
	555	0.42	0.02	43	311	0.64	-0.13	67	332	0.85	0.03	44	342	0.86	0.16	65	164	1100
C'	230	0.79	0.51	52	318	2.65	1.26	23	337	0.98	0.10	22	14	1.77	1.36	65	224	398
	425	0.68	0.45	329	168	3.08	2.72	280	228	1.57	1.13	292	275	2.55	1.85	343	36	398
Gentoo	24	0.39	0.07	354	230	0.84	0.28	8	334	0.59	0.13	340	273	0.32	0.23	280	267	335
	196	0.45	0.00	348	257	0.50	-0.05	330	312	0.39	0.00	334	284	0.21	0.10	280	49	335
	427	0.29	-0.15	22	263	0.48	0.01	324	286	0.43	0.12	344	281	0.14	0.08	302	293	335
	604	0.34	-0.01	29	269	0.45	0.02	270	228	0.32	-0.07	321	240	0.37	0.22	12	309	335
RSFE-C	241	0.73	-0.23	88	31	2.73	0.95	337	285	0.59	-0.17	54	89	0.91	-0.12	345	170	414
	498	1.32	-0.32	67	259	7.02	0.14	88	250	2.05	0.27	59	343	2.13	0.62	82	165	414
Emperor	107	0.60	-0.08	356	247	0.63	-0.09	344	322	0.71	0.01	332	264	0.26	0.06	316	256	700
	210	0.45	-0.13	358	248	0.61	-0.13	345	316	0.61	-0.04	340	273	0.32	0.07	331	275	700
	497	0.59	0.11	341	219	0.57	-0.06	327	291	0.50	0.00	343	262	0.11	0.06	15	261	359
	657	0.36	-0.23	352	258	0.50	-0.23	1	342	0.51	-0.28	78	10	0.39	0.08	22	257	333
A'/Adélie	40	0.40	-0.10	1	250	0.60	0.23	320	296	0.41	-0.05	344	268	0.33	0.09	303	267	702
	220	0.47	0.03	320	231	0.31	-0.12	318	308	0.47	-0.03	332	270	0.26	0.03	317	309	739
	770	0.37	-0.01	335	221	0.28	-0.09	324	282	0.44	-0.05	335	265	0.20	-0.03	66	83	2159
RSFE-A	241	0.17	0.05	355	309	0.14	0.01	305	2	0.10	-0.03	347	325	0.08	0.02	29	331	731
	740	0.09	0.03	313	26	0.31	0.09	56	337	0.16	0.09	340	39	0.14	0.00	58	234	648
Chinstrap	36	0.51	0.16	17	253	0.34	-0.17	333	288	0.30	-0.15	342	276	0.25	0.03	317	272	356
	210	0.49	-0.06	343	234	0.44	0.02	337	317	0.64	0.04	350	296	0.39	0.07	351	315	703
	813	0.46	-0.09	350	244	0.41	0.04	357	323	0.44	-0.07	330	262	0.23	0.03	67	337	344
Prism-J	40	0.33	0.12	72	266	0.57	0.19	26	338	0.72	0.32	39	17	0.27	-0.02	51	237	281
	780	0.30	-0.03	82	337	0.28	0.02	51	6	0.27	-0.13	41	300	0.11	0.06	67	324	277
K	200	0.19	0.06	21	151	0.22	0.04	17	245	0.10	0.08	72	210	0.16	0.05	51	184	733

Results

Large-scale currents

The large-scale circulation of the Ross Sea is characterized by relatively weak currents, with average speeds of less than 8 cm s⁻¹ except along the southern and western boundaries where an intensified boundary current reaches speeds about twice that (see Van Woert *et al.* 2003 for a full discussion of

the sub-tidal circulation). In the present tidal analysis these flows are negligible, though their presence may in fact affect the propagation of tidal energy and therefore play a role in the physics producing the observed tides.

Time-averaged tides

The time-averaged, harmonic tidal constituents (Foreman 1978) are listed in Tables III and IV in terms of semi-major and semi-minor axes of the current ellipses, ellipse orientation, and phase relative to Greenwich. As found elsewhere in the Ross Sea the principal solar diurnal tide (K_1) is the dominant constituent, followed next by the principal lunar diurnal tide (O_1). The maximum K_1 and O_1 tidal currents were observed at sites near the shelf break, consistent with model results (MacAyeal 1984) and observations from the Weddell Sea (Foldvik *et al.* 1990). The Ross Sea K_1 amplitude is comparable to values observed at the Weddell Sea shelf-break, but the Ross Sea O_1 tide is approximately a factor of two larger than observed in the Weddell Sea (Foldvik *et al.* 1990). At the southern sites tidal amplitudes are much weaker, with A'/Adélie and Chinstrap to the west being weaker yet than Emperor and Gentoo in the Ross Sea Polynya. With the exception of the noisy Q_1 component the diurnal tides are largely barotropic: the depth-averaged tide generally is about five times larger than the RMS vertical variability. Exceptions are found at moorings RSFE-A and RSFE-C; also, amplitudes diminish with depth at Pop and especially C' (see discussion section) and are smaller at the mid-depth mooring at Crackle.

At moorings near the Ross Ice Shelf (i.e. A'/Adélie, Gentoo, Emperor, and Prism moorings A, B, & C) the sense of rotation for the K_1 and O_1 tides is clockwise (negative sign on the minor axis; see Table III) or cyclonic, contrary to the general expectation for southern hemisphere tides. This is consistent with their deep-water locations next to the Ross Ice Shelf, where westward-propagating barotropic shelf waves tend to produce cyclonic motion on the deep

(north) side of the shelf edge and anti-cyclonic motion on the shallow (sub-ice) side (MacAyeal 1984). Moorings deployed just at the ice edge (Prism-D, Prism-E, Pop) show the contrasting anti-cyclonic polarization. More open sites like B', Chinstrap, and RSFE-B have the default anti-cyclonic polarization. The northern shelf edge sites (C' and RSFE-C) also have anti-cyclonically rotating diurnal tides, but their very strong currents indicate that this is due to the presence of additional shelf waves propagating along the shelf-break. These shelf-break waves appear in models of Ross Sea tides (Robertson *et al.* 1998, Padman *et al.* 2003) and at comparable locations in the Weddell Sea (Middleton *et al.* 1987, Foldvik *et al.* 1990, Robertson 2005).

The semi-diurnal tidal constituents are significantly weaker than the diurnal constituents at all sites, with values of less than 1.0 cm s^{-1} (Table IV). Moreover, these currents are also roughly a factor of 5–10 weaker than the semi-diurnal currents observed in the Weddell Sea (Foldvik *et al.* 1990). In general the semi-diurnal tides are not strongly barotropic. At the critical latitude, where the semi-diurnal tide frequency equals the inertial frequency, semi-diurnal tides can in theory produce significant vertical current structure (e.g. Furevik & Foldvik 1996). The multi-level moorings near the M_2 critical latitude in this study, B' and prism-J, do show vertical structure in the M_2 component. Interestingly other semi-diurnal components at these moorings show comparable vertical variations. Since the expected M_2 vertical structure is ultimately frictional in origin (a non-linear process) it is not unreasonable that other components should become involved.

Time-variable tides

A spectrum of currents in the diurnal band shows distinct peaks of tidal energy rising above a background continuum (Fig. 2). This background continuum contains broad-band phenomena such as wind-forced motion and internal waves that for our purposes constitute noise superimposed on the
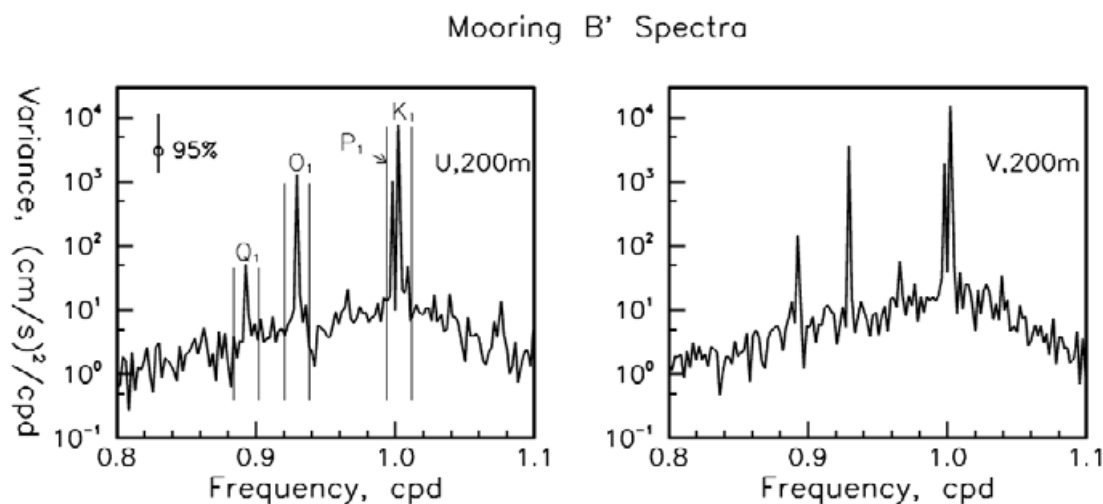

Mooring B' Spectra

Fig. 2. Diurnal-band spectra of 5 years of mooring B' velocities, showing the major tidal constituents and their 1/(56 day) width demodulation bands. 95% confidence limits are shown.
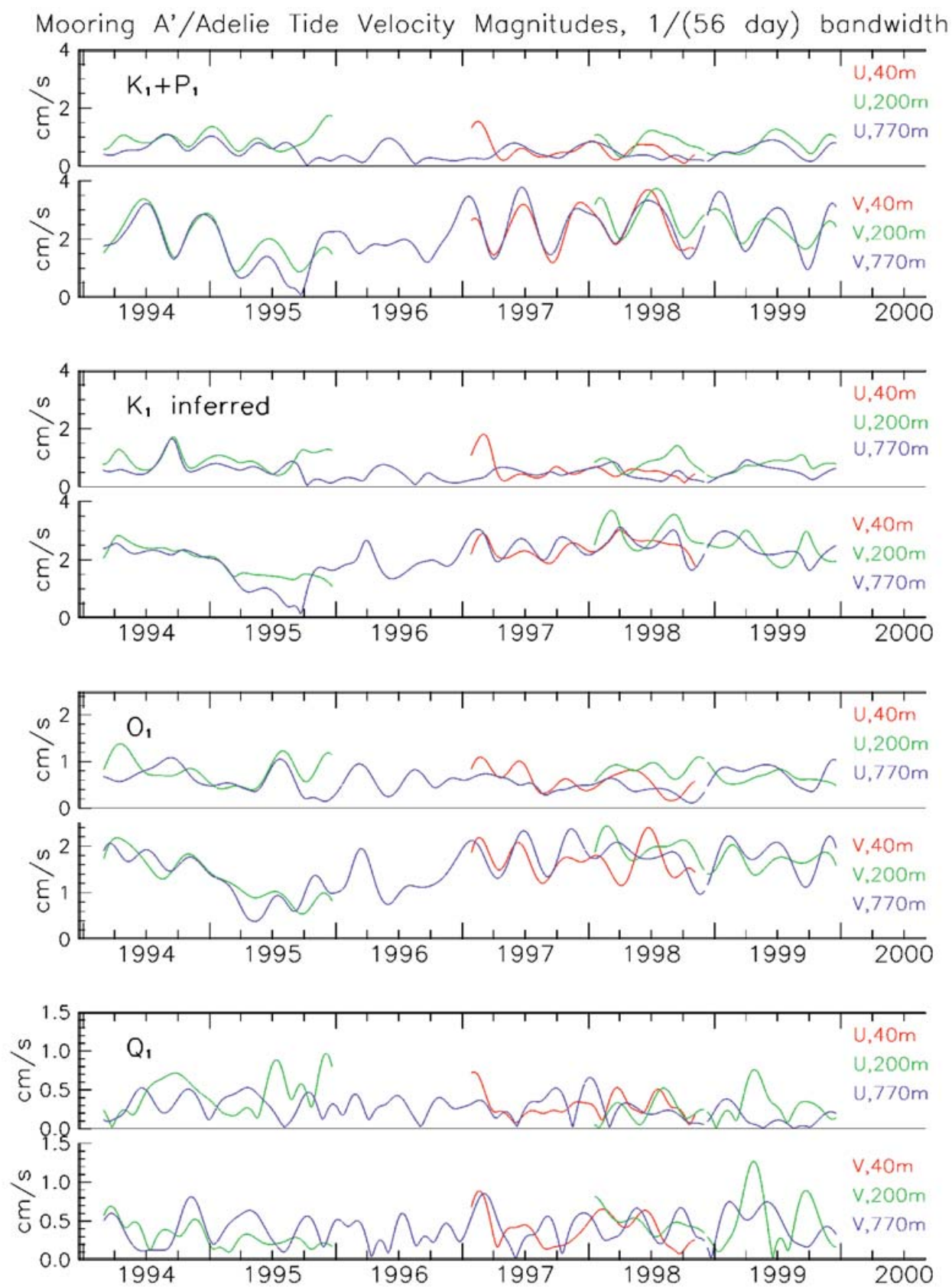
Fig. 3. 1/(56 day) bandwidth demodulated tide constituents at A'/Adélie, shown as magnitudes comparable to Table II. Note vertical scales vary between tide components. U and V refer to the eastward and northward velocity components.
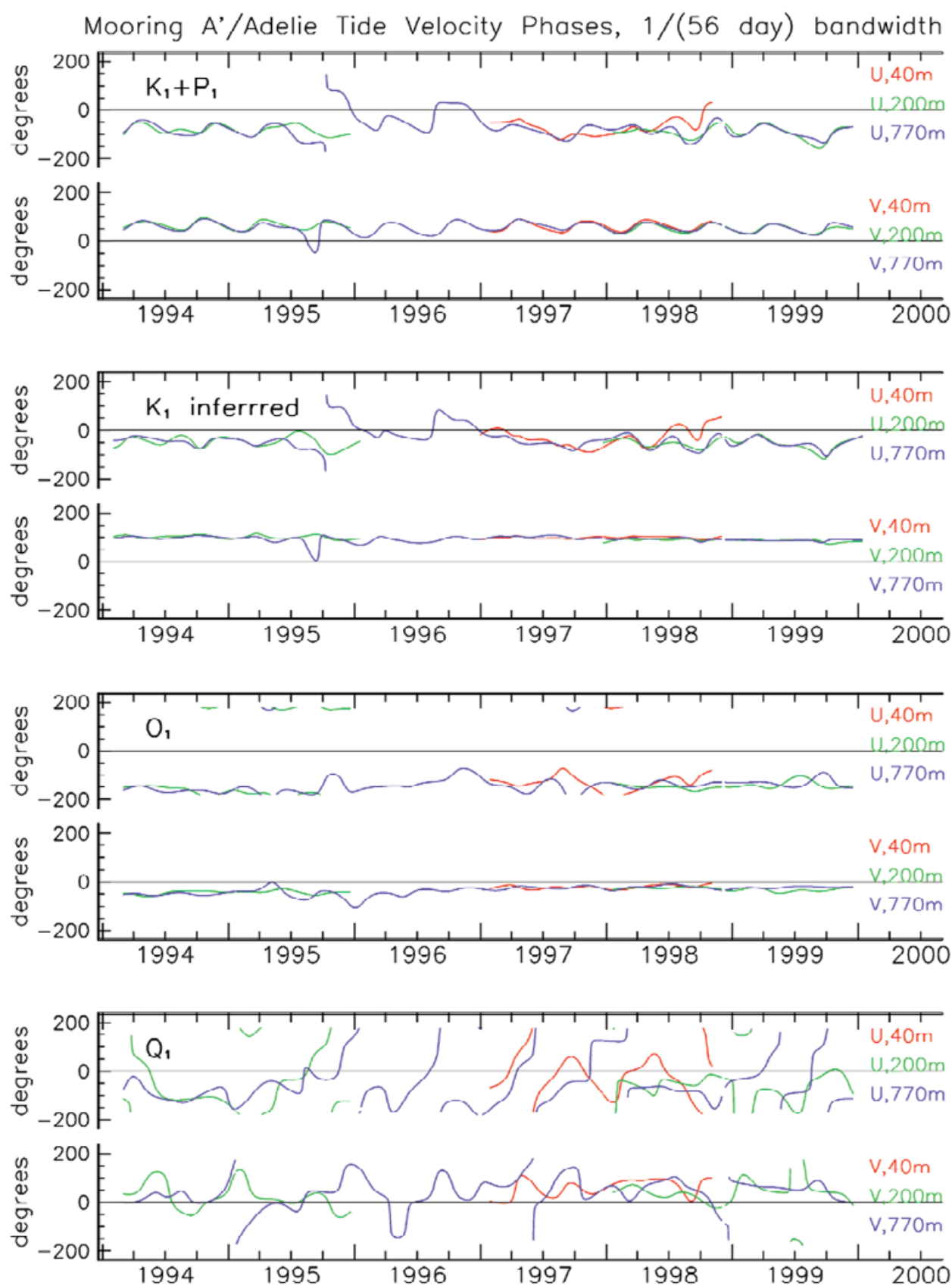
Fig. 4. As in Fig. 3 but for phase relative to the forcing frequency with arbitrary zero time.

tidal peaks. The tidal peaks themselves have finite width, indicative of energy tightly associated with the astronomical tide's line spectrum but displaced slightly away from that frequency by interaction with very low frequency variability (Munk *et al.* 1965) to produce a slow modulation of the underlying tide. In order to characterize this slow variability our complex demodulation analysis must at least separate the major tidal constituents. For present purposes this requires a frequency bandwidth no greater than $1/(28$ days), the separation between the Q_1 and O_1 components. K_1 and P_1 are not separable at periods less than 180 days: thus for this analysis we demodulate the combined K_1+P_1 band and isolate the K_1 component by inference (see below). We chose a bandwidth of $1/(56$ days) as being sufficient to capture all variability associated with the major tidal peaks while minimizing the noise contributed by the continuum (Fig. 2). A $1/(28$ day) analysis was also carried out for comparison, but provided no added insight to justify the greater noise level.

Demodulated time series for the K_1+P_1, O_1, and Q_1 bands at mooring A'/Adélie are shown in Figs 3 & 4. Series magnitude is scaled to represent the average velocity excursion and is comparable to the ellipse axis lengths in the harmonic analysis (Table III); phase represents the shift in tidal cycle timing relative to astronomical forcing (to within an arbitrary constant). A steadily changing phase would indicate some error in determining the astronomical forcing frequency, while fluctuations over time represent shifts in the tide relative to astronomical forcing. Note that this calculated phase is very sensitive to timing errors in the data: we added 5 hours to mooring B' data in years 1996 and 1997 to make these consistent with other years. While the combined K_1+P_1 band shows the characteristic twice-yearly beating of these constituents, both this and the O_1 band have substantial variability at interannual and other time scales as well. Their phases, on the other hand, are relatively stable. The Q_1 band is dominated by more random variability indicating that its lower amplitude is approaching the analysis noise level.

As mentioned, the proximity of the K_1 and P_1 constituent frequencies makes impossible an independent, quantitative estimate of the ocean's response to each: the dominant time variability is their beat cycle. Nevertheless with their frequencies so very close together it is reasonable to assume that the ocean responds similarly to each: that is, no conceivable oceanic process is expected to distinguish between the K_1 and P_1 forcing harmonics to any significant degree. Thus for our purposes we can treat the combined K_1+P_1 constituents as a single harmonic forcing that has slowly varying amplitude and phase, and inquire whether the ocean's response is in direct proportion to this varying forcing or if in fact it contains additional time variability. This is in exact analogy to our treatment of the O_1 and Q_1 components, but in those cases the forcing is uniform so that any observed variability from the demodulation sinusoid

can be attributed directly to the ocean's response. In the K_1+P_1 band we will in effect take the ocean's response to the combined forcing and re-scale it as though it were forced by K_1 alone.

We characterize the slowly varying K_1+P_1 forcing by finding for each velocity time series the best harmonic fit of the two astronomical forcing frequencies, resulting in two unvarying complex constants for each series. Since we've assumed uniform ocean physics across the K_1+P_1 band the ocean's response at these two frequencies should be in uniform proportion to the astronomical forcings. In verification of this, the observed relationship between the K_1 and P_1 response harmonics was extremely uniform at all depths and all moorings, except for slight degradations of signal by varying degrees of noise. Choosing the most robust example of K_1 and P_1 harmonics at each mooring we demodulate the combined harmonics to form a (complex) time series of K_1+P_1 forcing phase and amplitude at that mooring, essentially finding the slowly-varying astronomical forcing mentioned above (to within a constant complex factor representing the ocean's time-averaged response):

$$H_{K_1+P_1}(t)= \sum_{f=f_{K_1},f_{P_1}} e^{i(f-f_0)t} \left[\frac{\sqrt{2}}{T} \int_0^T u(\tau)e^{-if\tau}\,d\tau \right]. \quad (3)$$

We divide this forcing time series into the full demodulated ocean response time series (1) for the K_1+P_1 band (i.e. Fig. 3 top panel) to get a non-dimensionalized time series of response per unit forcing. For purposes of display and discussion we then re-dimensionalize this response time

Table V. The demodulated tidal constituents at selected moorings in terms of time-averaged magnitude and rms variability.

| | 1/(56 day) Bandwidth Tide Magnitudes | | | | | | | |
| | K_1+P_1 | | K_1 inferred | | O_1 | | Q_1 | |
MCM	mean	rms	mean	rms	mean	rms	mean	rms
adel040	2.37	1.06	2.47	0.58	1.75	0.52	0.36	0.42
adel200	2.31	1.05	2.38	0.83	1.71	0.63	0.38	0.51
adel770	2.09	1.10	2.12	0.77	1.58	0.71	0.32	0.44
chin037	1.70	0.75	1.78	0.36	1.40	0.37	0.23	0.32
chin208	2.23	0.86	2.32	0.29	1.68	0.29	0.35	0.27
chin814	1.52	0.72	1.61	0.34	1.24	0.33	0.24	0.19
empr041	2.70	1.15	3.22	0.34	2.41	0.49	0.41	0.67
empr105	3.75	1.59	3.93	0.70	2.24	0.67	0.55	0.70
empr212	3.53	1.52	3.67	0.62	2.29	0.70	0.60	0.69
empr495	3.30	1.47	3.53	1.28	2.03	0.59	0.58	0.69
gent030	3.41	1.43	3.55	0.51	2.43	0.52	0.55	0.50
gent200	4.15	1.40	4.36	0.39	2.91	0.52	0.77	0.56
gent431	3.37	1.15	3.59	0.42	2.33	0.30	0.48	0.52
gent609	3.23	1.19	3.42	0.23	2.22	0.21	0.57	0.28
b'200	9.72	3.96	10.1	1.73	4.52	0.88	0.91	0.55
b'548	7.95	3.69	8.13	1.55	3.92	1.01	0.86	0.48
rsfe-c241	22.36	5.74	22.45	2.18	23.28	3.13	2.09	1.85
rsfe-c498	16.91	5.9	16.88	2.65	15.82	2.02	3.36	1.19
c'200	46.66	17.63	47.82	2.79	43.51	4.86	6.16	1.65
c'416	27.92	8.73	28.96	3.91	23.99	6.76	2.55	1.01
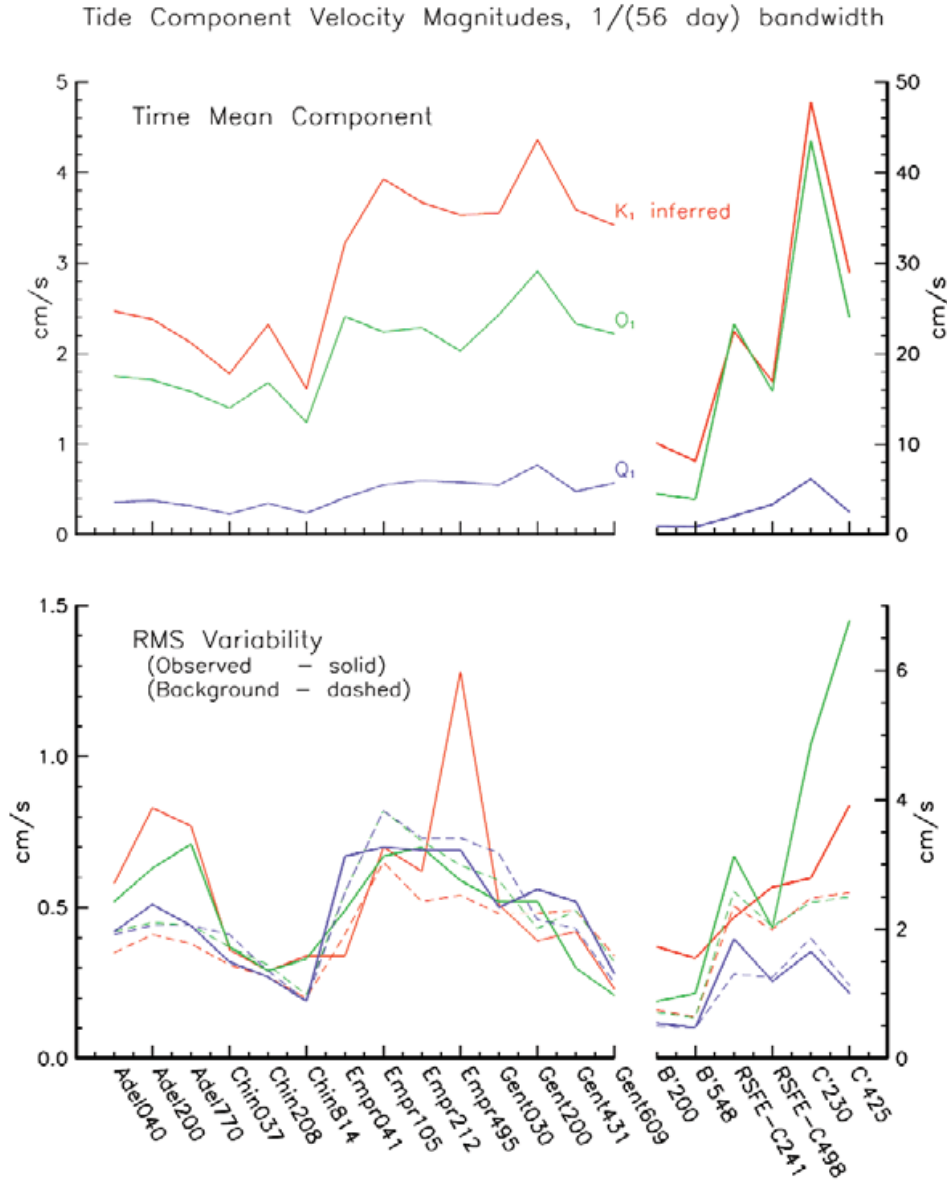
Fig. 5. The time-averaged magnitude and rms variability of demodulated tidal constituents (e.g. Figs 3 & 4). Note the rescaled velocity axis for the southern moorings on the left. Dashed lines denote the rms noise expected from the surrounding broadband spectral continuum (see text). Corresponding 95% confidence intervals for continuum-induced noise vary according to the amount of data at each instrument (Table III), but span 0.77 to 1.42 times the rms noise level for two years of data and 0.84 to 1.22 for five years.

series with the K_1 harmonic amplitude to get the inferred K_1 ocean response; that is, the response we would see from K_1 forcing alone:

$$D_{K_1}(t) = D_{K_1+P_1}(t)\frac{H_{K_1}}{H_{K_1+P_1}(t)}. \qquad (4)$$

This process substantially eliminates the K_1/P_1 time series beating (Fig. 3 first panel) to leave the ocean's time-varying response clear (Fig. 3 second panel). As with the O_1 component the phases of the inferred K_1 component are fairly stable: the greater part of the time variability appears in the amplitude time series. This held true in general at the other moorings with the exception of one month at the Emperor mooring, where O_1 phase lagged so rapidly as to throw much of its energy into the Q_1 band (not shown).

RMS Tide Component Variability

To summarize the demodulated tide results in quantitative form the mean and RMS time variability of the response in each band is presented in Table V and plotted in Fig. 5 for representative moorings around the Ross Sea Polynya to the south and near the shelf break to the north. Fig. 5 has two magnitude scales, one for the southern moorings on the left and another for the more energetic northern moorings on the right. To estimate the noise contributed by the background continuum (e.g. Fig. 2) we complex demodulated 1/(56 day) wide bands on either side of each tidal band and averaged together these two 'noise' bands to estimate the noise variance in the intervening tidal band. At several locations, notably A'/Adélie, B', C', and Emperor at 495 m depth, the RMS tide component variability rises well above the continuum noise floor and so is a candidate for variable
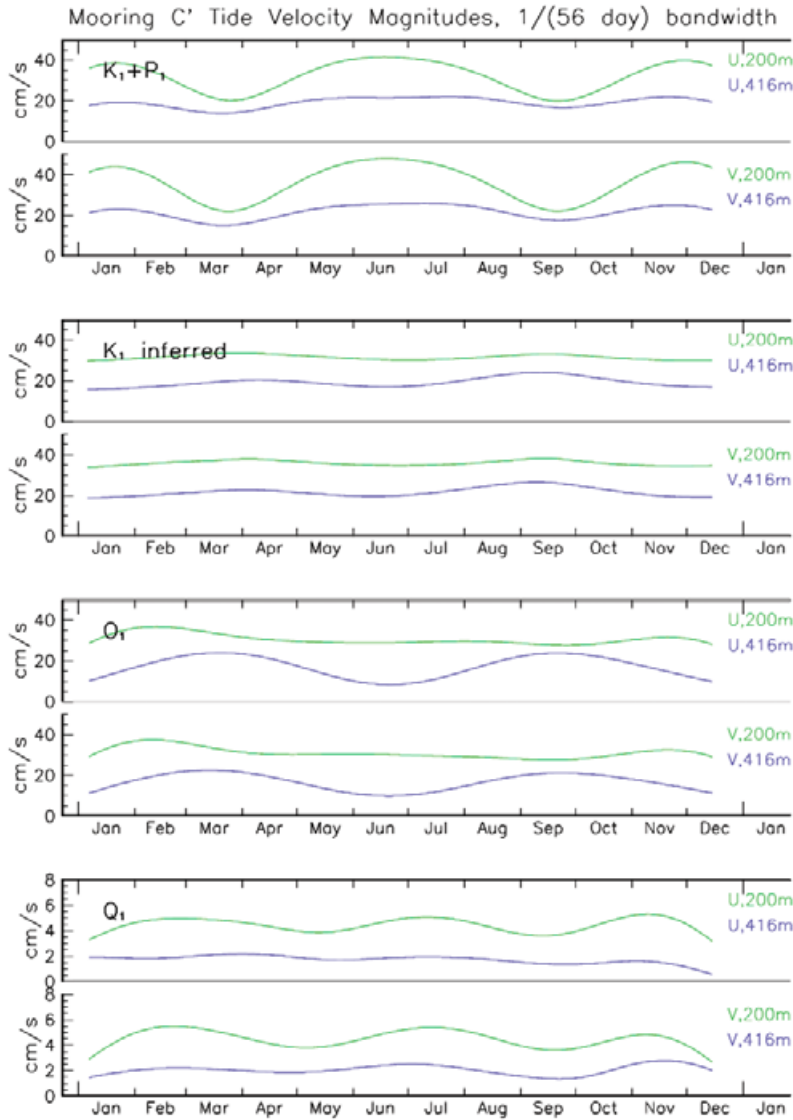
Fig. 6. 1/(56 day) demodulated tide constituent magnitudes at mooring C'.

ocean response to tidal forcing.

Discussion

RMS tidal component variability, noise or response

For purposes of assimilating local tide data into prediction models, the source of a tide component's time variability is largely irrelevant; whether noise or variable ocean response, the effect contributes uncertainty to the subsequent prediction that must be allowed for. Nevertheless we wish to further identify the physics of this variability, both for purposes of scientific understanding and in anticipation of including such physics in model simulations (e.g. Cummins *et al.* 2000's seasonal tide model). Here we distinguish between the two lowest-order possibilities, geophysical background noise and variable ocean response.

Geophysical background noise, contributed by wind forcing and other non-tidal motions, is assumed to be relatively broadband in nature: this is the spectral continuum mentioned previously. Given this assumption we expect relatively constant noise energy across the diurnal band, and further that the noise level of our analysis is roughly proportional to the selected bandwidth since this determines how much continuum noise is included. At many of the locations analysed (Fig. 5) the observed rms tidal instability is consistent with broadband noise: the variability is relatively uniform across tidal components and approximates the estimated noise levels. Further comparison between this 1/(56 day) bandwidth calculation and the 1/(28 day) calculation (not shown) demonstrates that the variability does in fact scale with bandwidth (not shown).

On the other hand, true ocean tidal instability involves a changing response to the astronomical forcing, perhaps through resonant shelf waves, changing stratification and background currents, non-linear interactions, etc. These actually scatter tidal energy over a broader range of frequencies, producing the spectral peak widths mentioned

earlier. For this case we expect the RMS variability of each tidal constituent not only to rise above the continuum noise level but to be roughly proportionate to that constituent's mean amplitude: that is, we expect the scattering physics to be uniform across the diurnal band (unless one imagines a very sharp resonance) and therefore to scatter energy from each constituent in proportion to that constituent's amplitude. Further, such variability should be relatively independent of the analysis bandwidth so long as this bandwidth includes the obvious tidal peak width. Several of the analysed moorings exhibit tidal instability as so defined: B' among the northern moorings and A'/Adélie among the southern. In particular Fig. 3 clearly shows the resolved tide components, K_1 and O_1, varying similarly in time consistent with our assumption of uniform scattering physics. In addition to these moorings, Emperor at 495 m depth and C' have enhanced time variability at specific tidal components. In general none of this variability scales significantly with bandwidth. Thus we can conclude with some confidence that all four examples are in fact unstable tide responses (though Emperor at 495 m is problematic, see below). From the values shown at A'/Adélie and C' it is clear that such instability can amount to fully a third of the underlying tide component's mean amplitude. Since adjacent moorings have dissimilar responses the spatial scales of such variability are in this case less than 100 km. Characterizing the time scales of the instability is difficult with so few

degrees of freedom; but all of the moorings having believable tide component instability showed clearly discernible variability at seasonal to interannual time scales (e.g. Fig. 3), indicating that the longer time scales are likely to be the more important.

Physics of tidal component instability

With isolated moorings in complicated bathymetry it is difficult to address the physical mechanisms of tidal component instability (e.g. Middleton *et al.* 1987, Padman *et al.* 1992). Nevertheless at Mooring C' on the shelf break it is clear that the tide component instability there is to a large degree frictional interaction with the bottom. At the deeper instrument the O_1 component and Q_1 components exhibit a twice-yearly modulation in sympathy with the K_1+P_1 tide variation (Fig. 6). From the velocity time series (Fig. 7) it is clear that a frictional benthic layer is present: deeper currents are severely limited in magnitude relative to the freer flow above, and are even clipped in the case of currents coming northward off the shallower shelf. Such severe non-linear interaction between tide components pose obvious complications in attempts to fit the data with the harmonics of a few major tidal components.

Tidal component variability at B' and A'/Adélie are due to different mechanisms: the changes there involve long term drifts in component amplitudes reminiscent of the seasonal
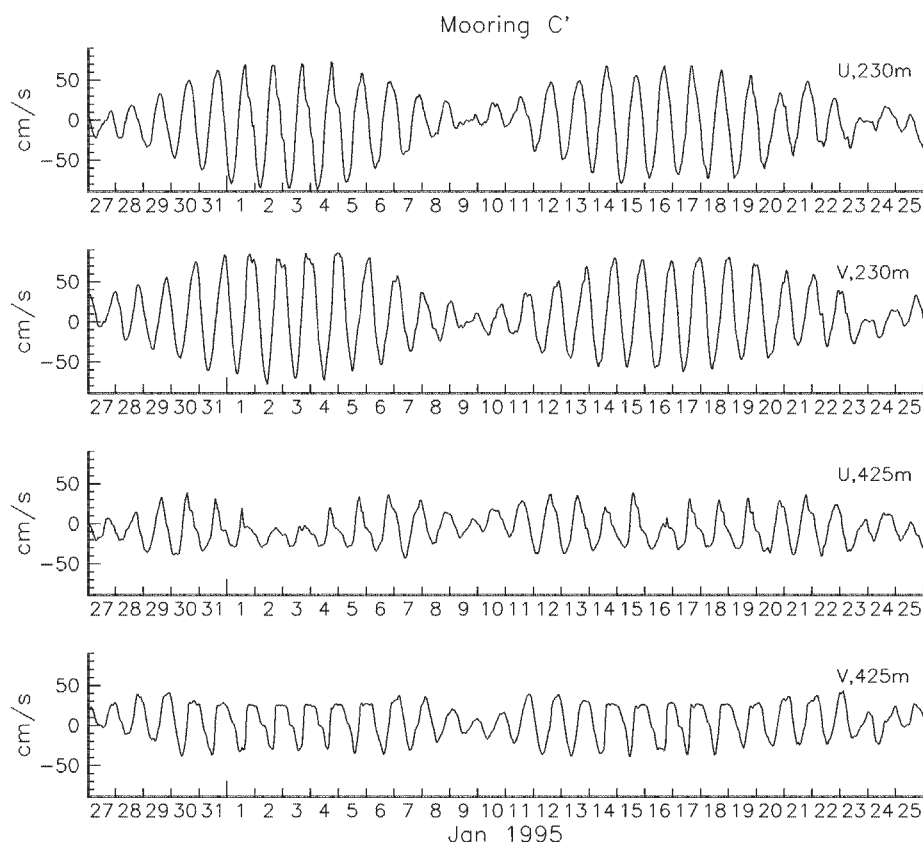

Fig. 7. A one-month time series of velocities at mooring C', in total water depth 456 m.

changes observed by Cummins *et al.* (2000). Some of the O_1 variability at A'/Adélie does appear correlated with the K_1+P_1 beat cycle, possibly through frictional interactions as above; but the dominant source of time variability for both O_1 and K_1 components is the longer-term drift during 1994–95. Determining whether these long-term changes can be attributed to changes in stratification and large-scale currents as off Vancouver Island (Cummins *et al.* 2000) probably requires a high-resolution tidal model and/or more data than are presently available. Nevertheless one useful observation is that the tidal component time variability occurs almost entirely in amplitude rather than phase. If tidal instability were due to changing propagation speed of the tide from its relatively distant forcing regions (as in Cummins *et al.* 2000) then one could reasonably expect variability in phase as well as amplitude. On the other hand if tidal instability were due to a varying local resonance (e.g. Middleton *et al.* 1987, Padman *et al.* 1992) then the tidal amplitude alone would change, with phase remaining synchronized with the forcing. Thus our results consistently favour the hypothesis that tidal instability in the Ross Sea is caused by changing local resonances that amplify the tidal response to varying degrees.

The Emperor mooring is anomalous in that instability focuses on a specific tidal component at a single depth (Fig. 5). The major source of this time variability comes from an increase in K_1 amplitude in the period September–October 1997, during which the K_1 phases remain steady. The flow throughout this period, however, is characterized by energetic (~20 cm s^{-1}) flows at various time scales (not shown) with no discernible relation to the K_1 tidal frequency. Thus it is difficult to rule out the possibility that non-tidal geophysical noise happened to concentrate in the K_1+P_1 band. Since this period occurs during a minimum of K_1+P_1 forcing the inferred K_1 amplitudes are 1.6 times greater than the observed K_1+P_1 variability: any geophysical noise during the period will be multiplied by the same factor, lending it artificial significance.

Analysis of the tides in terms of rotary rather than rectilinear velocities (not shown) generally reinforces the picture presented above. Tide component variability that represents a changing response (Adélie, B') tends to have the same polarization as the underlying time mean component, though this tendency is confused somewhat at the deeper Adélie instruments where K_1 variability looses some of its time mean clockwise polarization. In contrast tide component variability that doesn't exceed background noise levels tends to have little polarization compared to the time mean component, consistent with the variability in these cases being geophysical noise. Interestingly the anomalous K_1 variability at Emperor 495 m also shows very little polarization, though the time mean component is not so strongly polarized as to make this conclusive.

Van Woert *et al.* (2003) note that the Emperor bottom instrument (656 m) and others showed several intermittent periods during winter in which the tides largely disappeared. These periods were correlated with relatively weak currents at this and shallower levels, and so might be attributed to instrument malfunction such as the stalling of rotors. Nevertheless tides at other locations on the Antarctic continental shelf have been observed to cease during winter (Foldvik *et al.* 1990), and intermittent tidal bursts have been observed at other mid-latitude sites (Magaard & Key 1973). Foldvik *et al.* (1990) attributed this intermittency to a wintertime break down in the stratification; but Cummins *et al.* (2000) found that similar trapping of tides to the surface layer off Vancouver Island's shelf could only be replicated by introducing stratification into their model. Clearly the source of such intermittency remains a topic for further research. As a practical matter such periods of intermittency were excluded from our analysis since we rejected several year-long instrument records containing significant periods of low speed or restricted direction that might be construed as instrument malfunction. Thus while we may be reasonably sure that our results are not contaminated by instrument failure, we may also have excluded tidal physics of real interest.

Conclusions

Tides are the dominant source of currents in the Ross Sea, and can be an important mechanism for transporting sediments and vertically mixing nutrients and plankton through the water column. They also serve to obscure the Ross Sea's relatively weak large-scale circulation in all but the most heavily-averaged current measurements. To help characterize the tides and their effects we analysed the tides in the available current meter data from the Ross Sea. Consistent with previous studies the dominant constituents were the diurnal tides (K_1 and O_1); the semi-diurnal components and inertial currents were much weaker. The K_1 and O_1 tides were found to be strongest at the shelf-break and to decay in strength southwards. This is in broad agreement with both theory and previous observations from the Weddell Sea, and with models.

We also found significant time variability in the tidal response at a number of locations among both the northern moorings near the shelf-break and the southern moorings in and around the Ross Sea polynya. This instability in tidal response was significantly greater than the noise contributed by broad-band processes, and in the frequency domain can be thought of as a broadening of each tidal constituent's spectral peak. Complex demodulation of each constituent shows that at some moorings (B', A'/Adélie) the instability is relatively uniform across the diurnal band and roughly proportionate to each tide component's amplitude, while at other moorings (Emperor) the instability appears associated with a particular component and may in fact be due to noise. Adjacent (< 100 km distant) moorings may

exhibit little instability at all, indicating that the phenomenon's spatial scales are small as might be expected of topographic waves. The instability is almost entirely confined to amplitude variability rather than phase, suggesting that the instability is associated with changing local resonances rather than variable propagation speeds from distant forcing regions. Due to noise in the calculation the time scales of instability cannot be characterized with confidence, but much of the variability appears to be seasonal to interannual.

The rms time variability of a given tidal component can amount to as much as 1/3 of its mean amplitude. Thus tidal component instability poses substantial problems for attempts to characterize Ross Sea tides at the affected locations using data from either remote locations or disparate time periods. In such case accuracies better than 30% error cannot be achieved without some understanding of - and ability to model - the sources of tidal component instability.

Acknowledgements

References

BARRY, J.P. & DAYTON, P.K. 1988. Current patterns in McMurdo Sound, Antarctica and their relationship to local biotic communities. *Polar Biology*, **8**, 367–376.

CARMACK, E.C. 1977. Water characteristics of the Southern Ocean south of the Polar Front. *In* ANGEL, M. & DEACON, G., *eds. A voyage of discovery: 70th Anniversary volume. Supplement to Deep Sea Research.* New York: Pergamon Press, 15–42.

CARTWRIGHT, D.E. & RAY, R.D. 1990. Oceanic tides from GEOSAT altimetry, *Geophysical Research Letters*, **17** 619–622.

CRAWFORD, W.R. 1991. Tidal mixing and nutrient flux in waters of southwest British Columbia. *In* Parker, B.B., *ed. Tidal hydrodynamics*. New York: John Wiley & Sons, 885–869.

CUMMINS, P.F., MASSON, D. & FOREMAN, M.G.G. 2000. Stratification and mean flow effects on diurnal tidal currents off Vancouver Island. *Journal of Physical Oceanography*, **30**, 15–30.

DUNBAR, R.B., ANDERSON, J.B., DOMACK, E.W. & JACOBS, S.S. 1985. Oceanographic influences on sedimentation along the Antarctic continental shelf. *Antarctic Research Series*, **43**, 291–312.

EROFEEVA, S.Y., PADMAN, L. & EGBERT, G.D. 2005. Assimilation of ship-mounted ADCP data for barotropic tides: application to the Ross Sea. *Journal of Atmospheric and Oceanic Technology*, **22**, 721–734.

FOLDVIK, A., GAMMELSROD, T. & TØRRESEN, T. 1985. Ciculation and water masses on the southern Weddell Sea shelf. *Antarctic Research Series*, **43**, 5–20.

FOLDVIK, A., MIDDLETON, J.H. & FOSTER, T.D. 1990. The tides of the southern Weddell Sea. *Deep-Sea Research*, **37**, 1345–1362.

FOREMAN, M.G.G. 1977. *Manual for tidal heights analysis and prediction.* Pacific Marine Science Report 77–10. Patricia Bay, Victoria, BC: Institute of Ocean Sciences, 58 pp.

FOREMAN, M.G.G. 1978. *Manual of tidal current analysis and prediction*, Pacific Marine Science Report, 78–6. Patricia Bay, Sidney, BC: Institute of Ocean Sciences, 70 pp.

FUREVIK, T. & FOLDVIK, A. 1996. Stability at M2 critical latitude in the Barents Sea. *Journal of Geophysical Research*, **101**, 8823–8837.

LEFEVRE, F., LYARD, F.H., LE PROVOST, C. & SCHRAMA, E.J.O. 2002. FES99, a global tide finite element solution assimilating tide gauge and altimetric information. *Journal of Atmospheric and Oceanic Technology*, **19** 1345–1356.

LE PROVOST, C., LYARD, F., MOLINES, J.M., GENCO, M.L. & RABILLOUD, F. 1998. A hydrodynamic ocean tide model improved by assimilating a satellite altimeter-derived dataset. *Journal of Geophysical Research*, **103**, 5513–5529.

LEWIS, E.L. & PERKIN, R.G. 1985. The winter oceanography of McMurdo Sound, Antarctica. *Antarctic Research Series*, **43**, 145–165.

LODER, J.W. 1980. Topographic rectification of tidal currents on the sides of Georges Bank. *Journal of Physical Oceanography*, **10**, 1399–1416.

MACAYEAL, D.R. 1984. Numerical simulations of the Ross Sea tides. *Journal of Geophysical Research*, **89**, 607–615.

MACAYEAL, D.R. 1985. Tidal rectification below the Ross Ice Shelf, Antarctica. *Antarctic Research Series*, **43**, 109–132.

MAGAARD, L. & MCKEE, W.D. 1973. Semi-diurnal tidal currents at site "D". *Deep-Sea Research*, **20**, 997–1009.

MIDDLETON, J.H., FOSTER, T.D. & FOLDVIK, A. 1987. Diurnal shelf waves in the southern Weddell Sea. *Journal of Physical Oceanography*, **17**, 784–791.

MUNK, W., ZETLER, B. & GROVES, G.W. 1965. Tidal cusps. *Geophysical Journal*, **10**, 211–219.

MUNK, W. & WUNSCH, C. 1998. The moon and mixing: abyssal recipies II. *Deep-Sea Research*, **45**, 1977–2010.

PADMAN, L., PLUEDDEMANN, A.J., MUENCH, R.D. & PINKEL, R. 1992. Diurnal tides near the Yermak Plateau. *Journal of Geophysical Research*, **97**, 12 639–12 652.

PADMAN, L., EROFEEVA, L. & JOUGHIN, I. 2003. Tides of the Ross Sea and Ross Ice Shelf cavity. *Antarctic Science*, **15**, 31–40.

PILLSBURY, R.D. & JACOBS, S. 1985. Preliminary observations from long-term current meter moorings near the Ross Ice Shelf, Antarctica. *Antarctic Research Series*, **43**, 87–107.

ROBERTSON, R.A. 2005. Baroclinic and barotropic tides in the Weddell Sea. *Antarctic Science*, **17**, 107–120.

ROBERTSON, R., BECKMANN, A. & HELLMER, H. 2003. M₂ tidal dynamics in the Ross Sea. *Antarctic Science*, **15**, 41–46.

ROBERTSON, R., PADMAN, L. & EGBERT, G.D. 1998. Tides in the Weddell Sea. *Antarctic Research Series*, **75**, 341–369.

TSAI, P.T.H., O'BRIEN, J.J. & LUTHER, M.E. 1992. The 26-day oscillation observed in the satellite sea surface temperature measurements in the equatorial western Indian Ocean. *Journal of Geophysical Research*, **97**, 9605–9618.

VANNEY, J.R. & JOHNSON, G.L. 1985. GEBCO Bathymetric sheet 5.18 (Circum-Antarctic). *Antarctic Research Series*, **43**, 1–3.

VAN WOERT, M.L., JOHNSON, E.S., LANGONE, L., WORTHEN, D.L., MONAGHAN, A., BROMWICH, D.H., MELONI, R. & DUNBAR, R.B. 2003. The Ross Sea circulation during the 1990s. *Antarctic Research Series*, **78**, 5–34.

WILLIAMS, R.T. & ROBINSON, E.S. 1980. The ocean tides in the southern Ross Sea. *Journal of Geophysical Research*, **85**, 6689–6696.